Numerical Modeling and Simulation of Pile in Liquefiable Soil

Zhao Cheng[a], Boris Jeremić[b]

[a] *Staff Engineer, Earth Mechanics Inc. Oakland, CA 94621*
[b] *Associate Professor, Department of Civil and Environmental Engineering, University of California, Davis, CA 95616.*

Abstract

Presented in this paper is numerical methodology to model and simulate behavior of piles in liquefiable soils. Modeling relies on use of validate elasto-plastic material model for soil skeleton, verified fully coupled porous media (soil skeleton) – pore fluid (water) dynamic finite element formulation, and detailed load staging of FEM models. A bounding surface elastic–plastic sand model that accounts for fabric change is used to model soil skeleton, while a fully coupled, dynamic, inelastic formulation (u-p-U) is used to model soil and water displacement and pore water pressures. Much attention is paid to accurate staged loading of the models, which start from a zero state of stress and strain for a soil without a pile, followed by application of self weight, then by excavation and pile installation with application of pile self-weighting. Finally, seismic loading is applied followed by time to dissipate excess pore pressures that have developed. A total of six cases were modeled and simulated varying slope inclination, presence of pile–column and boundary condition for pile–column system. Presented are interesting and useful results that are used to deepen our understanding of behavior of soil–pile–column systems during liquefaction (lateral deformations, pile pinning effect, ground settlement). Moreover, detailed description of modeling is used to emphasize the availability and use of high fidelity modeling tools for simulating effects of liquefied soil on soil–structure systems.

Key words: elasto-plastic, fully coupled finite elements; liquefaction; soil–pile

*Corresponding Author: Boris Jeremić
Email addresses: `jeremic@ucdavis.edu` (Boris Jeremić)

dynamics;

1. Introduction

Liquefaction is one of the most complex phenomena in earthquake engineering. Liquefaction also represents one of the biggest contributors to damage of constructed facilities during earthquakes [Kramer, 1996]. Prediction of behaviors of liquefiable soils is difficult but achievable. There are number of methods that can be utilized to predict such behaviors. Methods currently used can have varying prediction accuracy and certainty. Of particular interest in this paper is the description of verified and validated numerical simulation methodology based on rational mechanics that is used to model, simulate and predict behaviors of a single pile in liquefiable soil subjected to seismic loading. Both level and sloping ground pile systems are modeled and simulated. Detailed description of background theory, formulation and implementation were recently given by Cheng et al. [2007] and Jeremić et al. [2008].

It should be noted that presented development do show great promise in analyzing a myriad of liquefaction related problems in geotechnical and structural engineering. The effectiveness and power of numerical simulation tools for analyzing liquefaction problems becomes even more important and prominent in the light of potential disadvantages of models used in experimental simulations. These disadvantages, related to proper scaling [Wood, 2004] and problems in maintaining appropriate similarities [Harris and Sabnis, 1999] for first order important phenomena, can render scaled models ineffective, when used for physical simulations (under one-step or multiple-step gravity loading).

In what follows, a brief literature review is provided. The literature review comprises sections on observations of liquefaction behavior in case studies, non–continuum modeling efforts, review of redistribution of voids and pore fluid volume/pressures phenomena and continuum modeling efforts.

Observation of Behavior.. Liquefaction behavior was observed during a number of earthquakes in the past. During Alaskan Earthquake (1964), liquefaction was the main cause of severe damage to 92 highway bridges, moderate to light damage to another

49 highway bridges, and moderate to sever damage to 75 railroad bridges [Youd and Bartlett, 1989]. During Niigata Earthquake (1964) liquefaction induced damage to foundation piles under Yachiya bridge [Hamada, 1992]. During that same earthquake, girders of Showa Bridge toppled as the support structure and piles moved excessively due to liquefaction [Japanese Society of Civil Engineers, 1966]. During Kobe Earthquake (1995), liquefaction was the primary cause of damage to many pile supported or caisson supported bridges and structures. For example, Shin–Shukugawa bridge was subjected to excessive pile foundation movement due to liquefaction [Yokoyama et al., 1997].

Opposed to these failures and collapses, there were a number of bridges with pile foundations that did not suffer much or even minor damage even though there was liquefaction around foundations. For example, pile foundations of the Landing Road Bridge in New Zealand performed quite well during Edgecumbe earthquake (1987) even with a significant liquefaction recorded [Berril et al., 1997, Dobry and Abdoun, 2001]. In addition to that, Second Maya Bridge piles (large steel pipes) were not damaged during Kobe earthquake despite significant liquefaction in surrounding soils [Yokoyama et al., 1997].

Non–Continuum Modeling Efforts.. Modeling and simulation of piles in liquefied grounds has been focus of a number of recent studies. The simple approach, based on scaling of p-y springs has been suggested early by Japanese Road Association [1980], Architectural Institutive of Japan [1988], Liu and Dobry [1995], Miura et al. [1989] and O'Rourke [1991]. However, large inconsistencies with material parameter selection are present when p-y spring approach is used for piles in liquefied soils. Since p-y methodology for liquefied soils is not based on rational mechanics, appropriate choice of material parameters is primarily based on empirical observations of behaviors of piles in liquefied soils in experimental studies. A number of experimental studies have carefully examined pile behaviors in liquefiable soils. We mention Tokida et al. [1992], Liu and Dobry [1995], Abdoun et al. [1997], Horikoshi et al. [1998] and Boulanger and Tokimatsu [2006]. Studies using physical model can be used to obtain very high quality data on behavior of piles in liquefied soils, provided that similarity of important physical phenomena is maintained [Wood, 2004, Harris and Sabnis, 1999]. Some of the recent papers that discussed use of these models and gave recommendations about parameter choices are listed for reference: Tokimatsu and Asaka [1998], Martin et al. [2002], Dobry et al. [2003], Liyanapathirana and Poulos [2005], Rollins et al. [2005], Čubrinovski and Ishihara [2006], Brandenberg et al. [2007].

Redistribution of Voids and Pore Fluid Volume/Pressures.. Mechanics of pile behavior in liquefiable grounds is based on the concept of redistribution of voids and pore fluid volume/pressures (RVPFVP). It should be emphasized that geomechanics phenomena of redistribution of voids – pore fluid volume/pressure is used here in purely mechanistic way. That is, RVPFVP is a phenomena that occurs in saturated soils and that phenomena is responsible for (is manifested in) liquefaction related soil behaviors with or without piles. This is noted as in some recent publications, RVPFVP terminology is explicitly used for problems of liquefaction induced failures of sloping grounds without piles. Our understanding of the RVPFVP phenomena is that RVFVP is responsible for many more facets of behavior of liquefied soils, rather than only failure of liquefied slopes.

The early investigation of the RVPFVP phenomena was related to the behavior of infinite slopes. For example, loss of shear strength in infinite slopes is one of the early understood manifestations of RVPFVP [Whitman, 1985, National Research Council, 1985, Malvick et al., 2006]. Laboratory investigation of sand was also used to observe the RVPFVP phenomena [Casagrande and Rendon, 1978, Gilbert, 1984]

Continuum Modeling Efforts.. Continuum based formulations for modeling liquefaction problems have been present for over two decades. In a landmark paper, Zienkiewicz and Shiomi [1984] presented three possible coupled formulations for modeling of soil skeleton – pore fluid problems. The most general and complete one is the so called u-p-U formulations while the other two, the u-p and the u-U have a number of restrictions on the domain of application. Here, the unknowns are the soil skeleton displacements u; the pore fluid (water) pressure p; and the pore fluid (water) displacements U. The u-p formulation captures the movements of the soil skeleton and the change of the pore pressure, and is the most simplistic one of the three mentioned above. This formulation neglects the differential accelerations of the pore fluid (it does account for acceleration of pore fluid together with soil skeleton, but not the separate one if it exists), and in one version neglects the compressibility of the fluid (assuming complete incompressibility of the pore fluid). In the case of incompressible pore fluid, the formulation requires special treatment of the approximation function (shape function) for pore fluid to prevent the volumetric locking [Zienkiewicz and Taylor, 2000]. The majority of the currently available implementations are based on this formulation. For example Elgamal et al. [2002] and Elgamal et al. [2003] developed an implementation of the u-p formulation with the multi-surface plasticity model by Prevost [1985], while Chan [1988] and Zienkiewicz et al. [1999] used generalized theory of plasticity Pastor et al. [1990].

The u-U formulations tracks the movements of both the soil skeleton and the pore fluid. This formulation is complete in the sense of basic variables, but might still experience numerical problems (volumetric locking) if the difference in volumetric compressibility of the pore fluid and the solid skeleton is large.

The u-p-U formulation resolves the issues of volumetric locking by including the displacements of both the solid skeleton and the pore fluid, and the pore fluid pressure as well. This formulation uses additional dependent unknown field of pore fluid pressures to stabilize the solution of the coupled system. The pore fluid pressures are connected to (dependent on) displacements of pore fluid. With known (given) volumetric compressibility of the pore fluid, pore fluid pressure can be calculated. Despite it's power, the u-p-U formulation has rarely been implemented into finite element code, and has never (at least to our knowledge) been used to analyze pile – liquefied soil interaction. This can be attributed in part to a sophistication of implementation that is required, and to a sizable increase in computational cost for u-p-U elements.

2. Numerical Formulation, Verification and Validation

2.1. Finite Element Formulation

The discretized, finite element system of equations for u-p-U formulation, which is based on earlier work by Zienkiewicz and Shiomi [1984], can be written in tensor index form

$$\begin{bmatrix} (M_s)_{KijL} & 0 & 0 \\ 0 & 0 & 0 \\ 0 & 0 & (M_f)_{KijL} \end{bmatrix} \begin{bmatrix} \ddot{\bar{u}}_{Lj} \\ \ddot{\bar{p}}_N \\ \ddot{\bar{U}}_{Lj} \end{bmatrix} + \begin{bmatrix} (C_1)_{KijL} & 0 & -(C_2)_{KijL} \\ 0 & 0 & 0 \\ -(C_2)_{LjiK} & 0 & (C_3)_{KijL} \end{bmatrix} \begin{bmatrix} \dot{\bar{u}}_{Lj} \\ \dot{\bar{p}}_N \\ \dot{\bar{U}}_{Lj} \end{bmatrix}$$

$$+ \begin{bmatrix} 0 & -(G_1)_{KiM} & 0 \\ -(G_1)_{LjM} & -P_{MN} & -(G_2)_{LjM} \\ 0 & -(G_2)_{KiL} & 0 \end{bmatrix} \begin{bmatrix} \bar{u}_{Lj} \\ \bar{p}_M \\ \bar{U}_{Lj} \end{bmatrix} + \begin{bmatrix} \int_\Omega N^u_{K,j}\sigma''_{ij}\mathrm{d}\Omega \\ 0 \\ 0 \end{bmatrix} - \begin{bmatrix} \bar{f}^u_{Ki} \\ 0 \\ \bar{f}^U_{Ki} \end{bmatrix} = 0 \tag{1}$$

where the components are

$$\begin{aligned}
(M_s)_{KijL} &= \int_\Omega N^u_K (1-n)\rho_s \delta_{ij} N^u_L \mathrm{d}\Omega \quad ; \quad (M_f)_{KijL} = \int_\Omega N^U_K n\rho_f \delta_{ij} N^U_L \mathrm{d}\Omega \\
(C_1)_{KijL} &= \int_\Omega N^u_K n^2 k^{-1}_{ij} N^u_L \mathrm{d}\Omega \quad ; \quad (C_2)_{KijL} = \int_\Omega N^u_K n^2 k^{-1}_{ij} N^U_L \mathrm{d}\Omega \\
(C_3)_{KijL} &= \int_\Omega N^U_K n^2 k^{-1}_{ij} N^U_L \mathrm{d}\Omega \quad ; \quad (G_1)_{KiM} = \int_\Omega N^u_{K,i} (\alpha - n) N^p_M \mathrm{d}\Omega \\
(G_2)_{KiM} &= \int_\Omega n N^U_{K,i} N^p_M \mathrm{d}\Omega \quad ; \quad P_{NM} = \int_\Omega N^p_N \frac{1}{Q} N^p_M \mathrm{d}\Omega \\
(\bar{f}_s)_{Ki} &= (f^u_1)_{Ki} - (f^u_4)_{Ki} + (f^u_5)_{Ki} \quad ; \quad (\bar{f}_f)_{Ki} = -(f_1)_{Ki} + (f_2)_{Ki} \\
(f^u_1)_{Ki} &= \int_{\Gamma_t} N^u_K \sigma''_{ij} r_j \mathrm{d}\Gamma \quad ; \quad (f^u_4)_{Ki} = \int_{\Gamma_p} N^u_K (\alpha - n) p r_i \mathrm{d}\Gamma \\
(f^u_5)_{Ki} &= \int_\Omega N^u_K (1-n)\rho_s b_i \mathrm{d}\Omega \quad ; \quad (f^U_1)_{Ki} = \int_{\Gamma_p} N^U_K n p r_i \mathrm{d}\Gamma \\
(f^U_2)_{Ki} &= \int_\Omega N^U_K n \rho_f b_i \mathrm{d}\Omega
\end{aligned} \tag{2}$$

Here N^u, N^p, N^U are shape functions of solid skeleton displacement, pore pressure and fluid displacement, respectively; ρ, ρ_s, ρ_f are density of the total, solid and fluid phases, respectively; n is porosity, the symbol r_i is the direction of the normal vector on the boundary; $\bar{u}_{Lj}$ are the nodal displacements of the solid part; $\bar{p}_M$ are the nodal pore pressures and $\bar{U}_{Lj}$ are the nodal displacements of the fluid part. Moreover, Ω represents the domain of interest; Γ_t is the traction boundary, and Γ_p is the pressure boundary. Set of dynamic Equations (1) represents the most general formulation and discretization for a material nonlinear (inelastic) porous medium (soil skeleton) that is fully saturated with linear elastic, compressible pore fluid (water).

Water accelerations are explicitly taken into account, both for conforming and differential movements with respect to the soil skeleton. This proves to be very important for models where porous soil is adjacent to structural foundations (piles for example). In these models, the dynamics of two model components, saturated soil and piles, are quite different and there exists a possibility of significant relative movement (displacements, velocities and accelerations) between soil skeleton and the concrete piles or footings. If this relative movement exists, pore water is pumped in and out of soil skeleton, thus creating a significant differential accelerations relative to the soils skeleton.

Both velocity proportional and displacement proportional damping follow directly from formulation and discretization. The velocity proportional damping is taken into account through damping matrix in Equation (1). Of particular interest are sub-matrices (tensors) $(C_1)_{KijL}$, $(C_2)_{KijL}$ and $(C_3)_{KijL}$ (Equations (2)). Physically, those sub-matrices represent coupling of pore water and solid skeleton, which is velocity proportional. This coupling is a function of permeability k and porosity n. For example, from Equation (2), it follows that for a soil with larger porosity n, which has more pores in a soil skeleton and therefore more pathways for pore water to travel through the soil, the damping will be higher. Similarly, for a soil with smaller permeability, where pore water has more difficulty in traveling through pores, where there is more friction of flowing pore fluid with the soil skeleton, the velocity proportional damping will be increased. Displacement proportional damping is controlled by inelastic material behavior, which in turn is controlled in the finite element discretization by the nonlinear, elastic–plastic stiffness matrix, given as $\int_\Omega N^u_{K,j} \sigma''_{ij} \mathrm{d}\Omega$ (see Equation (2)) here in order to correctly account for general, nonlinear dynamic time integration [Argyris and Mlejnek, 1991].

2.1.1. Time Integration

Numerical integration of Equations of motion (Equation 1) is done using Newmark [Newmark, 1959] or Hilber-Hughes-Taylor [Hilber et al., 1977, Hughes and Liu, 1978a,b] algorithms. Of particular importance is the proper algorithmic treatment for nonlinear analysis which introduces changes in a way residual forces are calculated

[Argyris and Mlejnek, 1991, Jeremić et al., 2008].

The finite element discretization in Equation (1) defines a damping matrix, which takes into account physics of velocity dependent interaction of pore water and soil skeleton. This damping matrix is more appropriately used here than damping matrix introduced through Rayleigh damping [Chopra, 2000]. It should be note that a small amount of numerical damping is used with both Newmark and Hilber-Hughes-Taylor methods, in order to damp out response in higher frequencies that is introduced by the spatial finite element discretization [Hughes, 1987].

2.1.2. Material Model

Material model plays one of the key roles in numerical simulation of the dynamic behaviors of liquefiable soil. Correct modeling of volumetric response by a good model on the constitutive level allows for accurate modeling of the boundary value problems where liquefaction is involved. In this work, a critical state soil mechanics based model developed by Manzari and Dafalias [1997] and Dafalias and Manzari [2004] is used. Among many excellent features of this model we note the capability to utilize a single set of material parameters for a wide range of void ratios and stress states for the same soil. This feature allows the same material parameters to be used from the very beginning of loading (from zero stress/strain state), through self weight, pile construction and finally dynamic shaking. In addition to that, model validation for Toyoura sand, used in this study, shows excellent agreement with test data [Jeremić et al., 2008]. It is emphasized again that Dafalias-Manzari set of models used here, together with powerful constitutive integrations, u-p-U formulation and proper dynamic equation of motion time integration [Jeremić et al., 2008], is capable to follow soil material from zero stress/strain state (before applying self weight) all the way to pre–liquefaction, liquefaction and post liquefaction behaviors. This transition

- from pre–liquefaction, where mean effective stress $p'(= -\sigma'_{kk}/3)$ is being continuously reduced (as pore water pressure is increased) to become numerically almost zero,
- through liquefaction, where mean effective stress p' is numerically almost zero,

- to post liquefaction, where mean effective stress p' is increasing (as pore water pressure is decreasing due to diffusion),

is successfully handled by the material model with the help of proper constitutive and dynamic level finite element integrations. Each of the above phases results in proper change (evolution) of the void ratio and the soil skeleton fabric, representing material internal variables.

2.2. Verification and Validation

Confidence in numerical prediction is firmly based on a valid process of verification and validation [Oberkampf et al., 2002]. Verification provides evidences that the model is solved correctly. Verification is also meant to identify and remove errors in computer coding and verify numerical algorithms and is desirable in quantifying numerical errors in computed solution. Validation provides evidences that the correct model is solved. It is custom to identify verification with mathematics of the problem and validation with the physics of the problem.

Computational simulation tools used in this study underwent detailed verification and validation program. Validation consisted of applying a comprehensive set of software verification tools, available in public domain and/or developed at the Computational Geomechanics Lab at UC Davis to developed libraries and programs. In addition to that, a number of closed form solutions were used to verify that our models were solved correctly. A set of problems with solutions developed by Coussy [1995] were numerically modeled and simulated during validation process [Jeremić et al., 2008]. Mentioned are verification problems of 1D consolidation, line injection of fluid in a reservoir, and cavity expansion in saturated medium (2D and 3D).

In addition to those problems which dealt with relatively slow phenomena without significant influence of inertial forces, a truly dynamic problem of shock wave propagation in porous medium was also used for verification [Gajo, 1995, Gajo and Mongiovi, 1995]. Verification examples using shock wave propagation are most sever tests of the u-p-U formulation and the numerical integration algorithms for the dynamic equations of motions. It should be noted that these verification test provided excellent, close matching of numerical and closed for solutions, within the known limitations of numerical accuracy of finite element discretization. This limitation in accuracy is a simple and expected consequence of approximate nature of the finite element method [Zienkiewicz and Taylor, 1991a,b], and the finite precision arithmetic used in computer calculations [Dennis and Schnabel, 1983].

Validation was done by simulating constitutive behaviors of sand material used in predictions (Toyoura sand). Comparison of validation predictions with physical test data [Jeremić et al., 2008] shows very good predictive capabilities of the material model as well as of the underlying numerical integration algorithms on the constitutive level.

3. Staged Simulation Model Development

Model development for a pile in the liquefiable soil follows physics (mechanics) of the problem as close as possible. Numerical simulation of such problems in geomechanics is usually based on stages of loading and increments within those stages.

All load stages are applied to a series of finite element models, all of which share features of an initial soil model. This initial soil model consists of a soil block with dimension of $12 \times 12 \times 15$ m (length $\times$ width $\times$ depth). Due to the symmetry of the model, only half of the block is modeled. Symmetry assumptions is based on assumption that all the loads, dynamic shaking and other influences are symmetric with respect to the plane of symmetry. This specialization to symmetric model reduces model generality (for example this use of symmetry will preclude analysis of dynamic shaking perpendicular to sloping ground dip). However, as our goal is to present a methodology of analyzing behavior of piles in liquefying ground, this potential drawback is not deemed significant in this study. Finite element mesh for the model is presented in Figure (1). The initial mesh consists of 160 eight node u-p-U elements.

Each node of the mesh has 7 degrees of freedom, three for soil skeleton displacements (u_i), one for pore water pressure (p), and three for pore water displacement (U_i). While it can be argued that the mesh is somewhat coarse, it is well refined around the pile, yet to be installed, in place of gray region in the middle.

A single set of parameters is used with the Dafalias-Manzari material model. Soil is modeled as Toyoura sand and material parameters (summarized in Table 3) are calibrated using tests by Verdugo and Ishihara [1996], while initial void ration was set

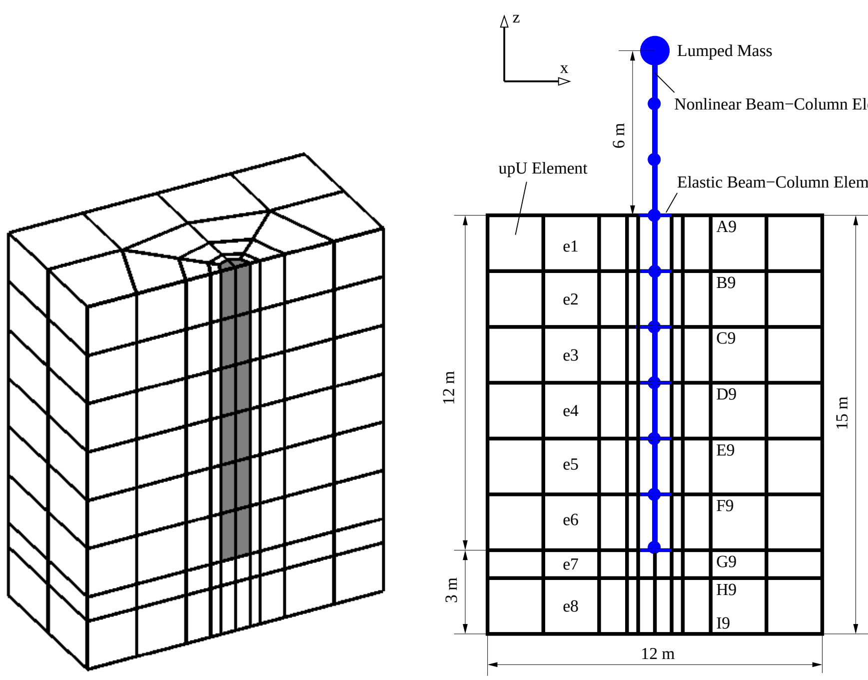

Figure 1: Left: Three dimensional finite element mesh featuring initial soil setup, where all the soil elements are present. The gray region of elements is excavated (numerically) and replaced by a pile during later stages of loading; Right: Side view of the pile-soil model with some element and node annotation, used to visualize results.

Table 1: Material parameters used for Dafalias-Manzari elastic–plastic model.

Material Parameter		Value	Material Parameter		Value
Elasticity	G_0	125 kPa	Plastic modulus	h_0	7.05
	v	0.05		c_h	0.968
Critical sate	M	1.25		n_b	1.1
	c	0.8	Dilatancy	A_0	0.704
	λ_c	0.019		n_d	3.5
	ξ	0.7	Fabric-dilatancy	z_{max}	4.0
	e_r	0.934		c_z	600.0
Yield surface	m	0.02			

Table 2: Additional parameters used in FEM simulations.

Parameter		Value
Solid density	ρ_s	2800 kg/m^3
Fluid density	ρ_f	1000 kg/m^3
Solid particle bulk modulus	K_s	1.0×10^{12} kN/m^2
Pore fluid bulk modulus	K_f	2.2×10^6 kN/m^2
permeability	k	1.0×10^{-4} m/s
Gravity	g	10 m/s^2

to $e_0 = 0.80$. It is very important to emphasize that the state of stress and internal variables from initial state (zero for stress and given value for void ratio and fabric) will evolve through all stages of loading by proper modeling and algorithms, by using single set of material parameters. Table 2 presents additional parameters, other than material parameters presented in Table 3, used for numerical simulations.

3.1. First Loading Stage: Self Weight

The initial stage of loading is represented by the application of self weight on soil, including both the soil skeleton and the pore water. Initial state in soil before application of self weight is of a zero stress and strain while void ratio and fabric are given initial values. The state of stress/strain, void ratio and fabric will evolve upon application of self weight. At the end of self weight loading stage, soil is under appropriate state of stress (K_0 stress), the void ratio corresponds to the void ratio after self weight (redistributed such that soil is denser at lower layers), while soil fabric has evolved with respect to stress induced anisotropy. All of these changes are modeled using

Dafalias–Manzari material model and using constitutive and finite element level integration algorithms developed within UC Davis Computational Geomechanics group in recent years.

Boundary conditions (BC) for self weight stage of loading are set in the following way:

- Soil skeleton displacements (u_i), are fixed in all three directions at the bottom of the model. At the side planes, nodes move only vertically to mimic self-weight effect. All other nodes are free to move in any direction.

- Pore water pressures (p), are free to develop at the bottom plane and at all levels of the models except at the top level at soil surface where they are fixed (set to zero, replicating drained condition),

- Pore water displacements (U_i), are fixed in all three directions at the bottom, are free to move only vertically at four sides of the model and are free to move in any direction at all other nodes.

These boundary condition are consistent with initial self-weighting deformation condition for soil and pore water at the site.

For the case of sloping ground, an additional load sub-stage is applied after self weight loading, in order to mimic self weight of inclined (sloping) ground. This is effectively achieved by applying a resultant of total self weight of the soil skeleton times the sine of the inclination angle at uphill side of the model. This load is applied only to the solid skeleton DOFs, and not on the water DOFs. Physically it would be correct to consider the sloping ground effects on the pore water as well. This will create a constant flow field of the water downstream, which, while physically accurate, is small enough that it does not have any real effect on modeling and simulations performed here.

3.2. Second Loading Stage: Pile–Column Installation

After the first loading stage, comprising self weight applications (for level or sloping ground, as discussed above), second loading stage includes installation (construction) of the pile–column. Modeling changes performed during loading stage included:

- Excavation of soil occupying space where the pile will be installed. This was done by removing elements, nodes and loads on elements shown in gray in Figure (1).

- These elements were replaced by very soft set of elements with small stiffness, low permeability. This was done in order to prevent water from rushing into the newly opened hole in the ground after original soil elements (used in the first loading stage) are removed.

- Installation of a pile in the ground and a superstructure (column) above the ground. Nonlinear bean–column elements were used for both pile and column together with addition of appropriate nodal masses at each beam-column node, and with the addition of a larger mass at the top representing lumped mass of a bridge superstructure. Pile beam-column elements were connected with soil skeleton part of soil elements using a specially devised technique.

As mentioned earlier, the volume that would be physically occupied by the pile in the pile hole, is "excavated" during this loading stage. Beam–column elements, representing piles, are then placed in the middle of this opening. Pile (beam–column) elements are then connected to the surrounding soil elements by means of stiff elastic beam–column elements. These "connection" beam–column elements extend from each pile node to surrounding nodes of soil elements. The connectivity of nodes to soil skeleton nodes is done only for three beam–column translational DOFs, while the three rotational DOFs from the beam–column element are left unconnected. These three DOFs from the beam–column side are connected to first three DOFs of the u-p-U soil elements, representing displacements of the soil skeleton (u_i). Water displacements (U_i) and pore water pressures (p) are not connected in any way. Rather, these two sets of DOFs representing pore water behave in a physical manner (cannot enter newly created hole around pile beam–column elements) because of the addition of a soft, but very impermeable set of u-p-U elements, replacing excavated soil elements. By using this method, both solid phase (pile with soil skeleton) and the water phase (pore water within the soil) are appropriately modeled. Figure (2) shows in some detail schematics of coupling between the pile and soil skeleton part finite elements.

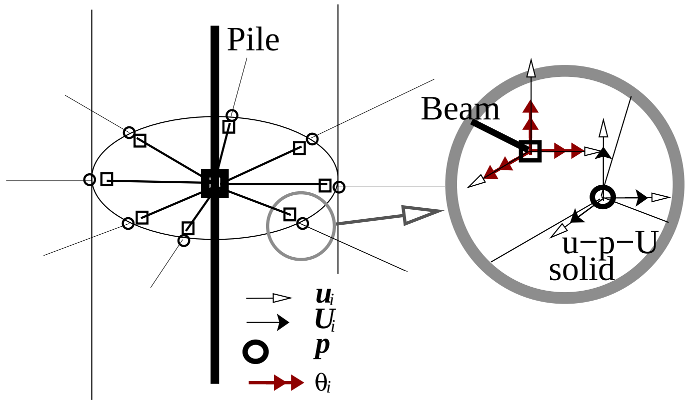

Figure 2: Schematic description of coupling of displacement DOFs (u_i) of beam-column element (pile) with displacement DOFs (u_i) of u-p-U elements (soil).

Nonlinear force based beam–column elements [Spacone et al., 1996a,b] were used for modeling the pile–column. Pile was assumed to be made of aluminum. This was done in order to be able to validate simulations with centrifuge experiments (when they become available). Presented models were all done in prototype scale, while for (possible future) validation, select results will be carefully scaled and compared with appropriate centrifuge modeling. Pile and the column were assumed to have a diameter of $d = 1.0$ m, with Young's modulus of $E = 68.5$ GPa, yield strength $f_y = 255$ kPa, and the density $\rho = 2.7$ kg/m^3. Wall thickness of prototype pile–column is $t = 0.05$ m. Lumped mass of pile and column was distributed along the beam–column nodes, while an additional mass was added on top ($m = 1200$ kg) that represents (small) part of the superstructure mass. This particular mass ($m = 1200$ kg) comes from a standard (scaled up in our case) centrifuge model for pile–column–mass used at UCD.

Figure (1) (right side) shows side view of the column-pile-soil model after second stage of loading.

3.3. Third Loading Stage: Seismic Shaking

After the application of self weight on the uniform soil profile, excavation and construction of the single pile with column and super structure mass on top and application of their self weight, the model is at the appropriate initial state for further application of loading. In this case, this additional loading comprises seismic shaking. For this stage, fixed horizontal DOFs used on the side planes during the first stage are removed (set free).

The input acceleration time history, shown in Figure (3) was taken from the recorded horizontal acceleration of Model No.1 of VELACS project Arulanandan and Scott [1993] by Rensselaer Polytechnic Institute (`http://geoinfo.usc.edu/gees/velacs/`). The magnitude of the motion is close to 0.2 g, while main shaking lasts for about 12

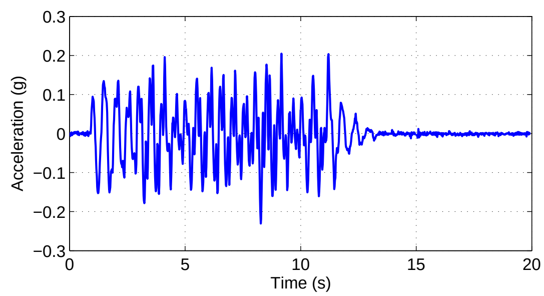

Figure 3: Input earthquake ground motions.

seconds (from 1 s to 13 s). Although the input earthquake motions lasts until approx. 13 seconds, simulations are continued until 120 seconds so that both liquefaction (dynamic) and pore water dissipation (slow transient) can be appropriately simulated during and after earthquake shaking [Jeremić et al., 2008].

3.4. *Free Field, Lateral and Longitudinal Models*

Six models were developed during the course of this study. First three models (model numbers I, II and III) were for level ground, while last three models (model numbers IV, V, and VI) were for sloping ground. First in each series of models (model I for level ground and model IV for sloping ground) were left without the second loading stage, without a pile–column system. Other four models (numbers II, III, V and VI) were analyzed for all three loading stages. Second in each series of models (models number II and V) had all displacements and rotations of pile–column top (where additional mass representing superstructure was placed) left free, without restraints. Thus, these two models represent lateral behavior of a bridge. Third in each series of models (model numbers III and VI) had rotations in *y* directions fixed at the pile–column top, thus representing longitudinal behavior of a bridge. Modeling longitudinal behavior of a bridge by restraining rotations perpendicular to the bridge superstructure is appropriate if the stiffness of a bridge superstructure is large enough, which in this case it was, as it was assumed to be a post–tensioned concrete box girder, so that realistically, the top of a column does not rotate (much) during application of loads. Table 3 summarizes models described above.

Table 3: Cases descriptions.

Case	Model sketch	Descriptions
I	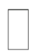	horizontal ground, no pile
II	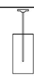	horizontal ground, single pile, free column head
III	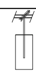	horizontal ground, single pile, no rotation at column head
IV		sloping ground, no pile
V		sloping ground, single pile, free column head
VI		sloping ground, single pile, no rotation at column head

4. Simulation Results

4.1. Pore Fluid Migration

Figures (4) through (6) show the Ru time history for up to 30 seconds, for elements (at one of Gauss point) e1, e3, e5 and e7 (refer to right side of Figure (1)). It is important to note that R_u is defined as the ratio of the difference of initial mean and current mean effective stresses over the initial mean effective stress:

$$R_u = \frac{p'_{initial} - p'_{current}}{p'_{initial}}$$

where mean effective stress is defined as $p' = \sigma'_{kk}/3$. This is different from traditional definition for R_u, that uses ratio of excess pore pressure over the initial mean effective stress ($p'_{initial}$). However, these two definitions are essentially equivalent, as soil is in the state of liquefaction for $R_u = 1$ (so that $p'_{current} = 0$), while there is no excess pore pressure for $R_u = 0$ (so that $p'_{initial} = p'_{current}$). However, the former definition is advocated here as it avoids the interpolation of pore pressure or extrapolation of the stresses (as the latter definition requires), since for the u-p-U element, stresses are available at Gauss points while pore pressures are available element nodes. In

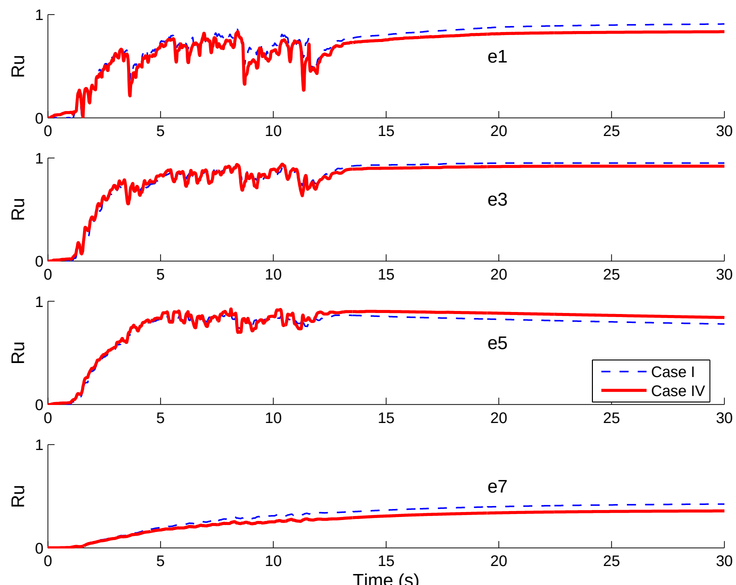

Figure 4: R_u times histories for elements e1 (top element), e3, e5, and e7 (bottom element) Gauss point) for Cases I (level ground, no pile) and IV (sloping ground, no pile).

particular, Figure 4 shows R_u time histories for four points for models I (level ground without pile) and model IV (sloping ground without pile). It is noted that differences are fairly small. It is interesting to observe that lower layers do not liquefy as supply of pore fluid for initial void ratio of $e_0 = 0.8$ is too small, and the pore fluid dissipation upward seems to be to rapid. On the other hand, the upper soil layers do reach close to or liquefaction state ($R_u = 1$). This is primarily due to the propagation of pore fluid pressure/volume from lower layers upward (pumping effect) and, in addition to that, to a local excess pore fluid production. These results can also be contrasted with those of Jeremić et al. [2008], where similar pumping scenario has been observed. The main difference between soil used by Jeremić et al. [2008] and here is in the coefficient of permeability. Namely, here $k = 1.0 \times 10^{-4}\ m/s$ was used [Čubrinovski et al., 2008, Uzuoka et al., 2008] while Jeremić et al. [2008] used $k = 5.0 \times 10^{-4}\ m/s$. It is important to note that other values of permeability for Toyoura sand have also been reported [Sakemi et al., 1995], but current value was chosen based on Čubrinovski [2007 –].

In addition to that, similar to Jeremić et al. [2008], sloping ground case shows larger R_u spikes, since there is static shear force (stress) that is always present from gravity load on a slope. This static gravity on a slope will result in an asymmetric horizontal shear stresses in the down–slope direction during cycles of shaking. This asymmetric shear stress induces a more dilative response for down–slope shaking which will help soil regain its stiffness in the dilative parts of the loading cycles. This observation can be used to explain smaller R_u spikes for the sloping ground case. Of course, this asymmetry in loading will result in larger accumulation of down–slope deformation.

While R_u ratios for level and sloping ground cases are fairly similar along the depth of the model, the response changes when the pile is present. Figure (5) shows R_u responses at four different points (along the depth) approximately midway between the pile and the model boundary, in the plane of shaking (see location of those elements in Figure (1) on page 11). In comparison to behavior without the pile (Figure (4)), it is immediately obvious that addition of a pile with a mass on top reduces R_u during shaking for the top element (e1). This is to be expected as presence of a pile–column–mass (PCM) system changes the dynamics of the top layers of soil significantly enough to reduce total amount of shear. This is particularly true for the top layers of soil as effects of column–mass tend to create compressive and extensive movements (compression when the PCM system moves toward soil and extension, and possibly even tension, when PCM system moves away from soil). However, this extension, or possible tension, is not directly observable in presented plots since array of elements where we follow R_u (e1, e3, e5, e7) is some distance away from the pile–soil interface. Middle layers (e3 and e5), on the other hand, display similar response to that of Cases I and IV, as shown in Figure (4). It is noted that in a case with of sloping ground with pile, the R_u measurements are always larger that those for level ground (this is also observed for Cases III and VI, as shown in Figure (6)). This is expected as presence of a pile in loose sand, and particularly the dynamic movement of a pile during seismic shaking, create an additional shearing deformation field (in the soil adjacent to the pile) that provides for additional (faster) compression of soil skeleton and thus creates additional volume of pore fluid, that is then distributed to adjacent soil (adjacent to the pile).

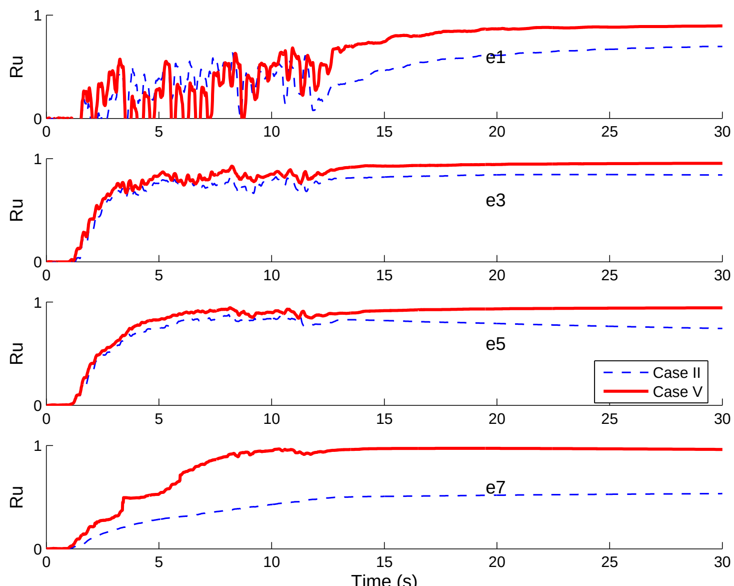

Figure 5: R_u times histories for elements e1, e3, e5, and e7 (upper Gauss point) for Cases II (level ground, with pile–column, free column head) and V (sloping ground, with pile–column, free column head).

Particularly interesting are R_u results for soil element e7, which is located below pile tip level (see Figure (1)). Observed R_u for Case V in element e7 is significantly larger than for the same element for Case II. Similarly, simulated R_u is larger than what was observed in cases without a pile (see bottom of Figure (4)). This increase in R_u for Case V (sloping ground with pile) is explained by noting that the pile "reinforces" upper soil layers and thus prevents excess shear deformation in the upper 12.0 m of soil (above pile tip). The reduction of deformation in upper layers of soil (top 12.0 meters) results in transfer of excessive soil deformation to soil layers below pile tip (where element e7 is located). This, in turn, results in a much larger and faster shearing of those lower loose soil layers. This significantly larger shearing results in a much higher R_u. Deformed shape, shown in Figure (7) for Case V, reinforces this explanation, showing much large shearing deformation in lower soil layers, below pile tip. Same observation can be made for Case VI, shown in Figure (7).

Observation similar to the above, for Cases II and V can be made for Cases III and

VI, results for which are shown in Figure (6). One noticeable difference in R_u results

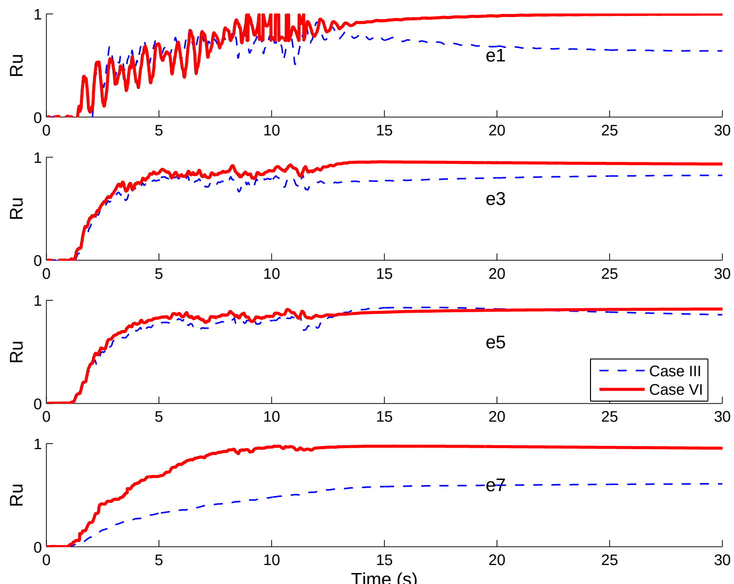

Figure 6: R_u times histories for elements e1, e3, e5, and e7 (upper Gauss point) for Cases III (level ground, with pile, no rotation of pile head) and VI (sloping ground, with pile-column, no rotation of column head).

between cases with free column head (Cases II and V) and cases with fixed rotation column head (Cases III and VI) is in significantly larger (and faster) development of R_u close to soil surface for a stiffer, no rotation column cases (Cases III and VI). This much larger R_u observed in a "stiffer" PCM system setup, is due to larger shearing deformation that develops in soils adjacent to the pile during shaking. The stiffer PCM system can displace less (because of additional no rotation condition on column top) while the soil beneath is undergoing shaking (same demand in all cases), thus resulting in larger relative shearing of soil, which then results in larger and faster pore pressure development close to the soil surface, where the column no rotation effect is most pronounced.

4.2. Soil Skeleton Deformation

A number of deformation modes is observed for both level and sloping ground cases, with or without PCM system. Figure (7) shows deformation patterns and excess pore pressures in symmetry plane for all six cases over a period of eighty seconds. A

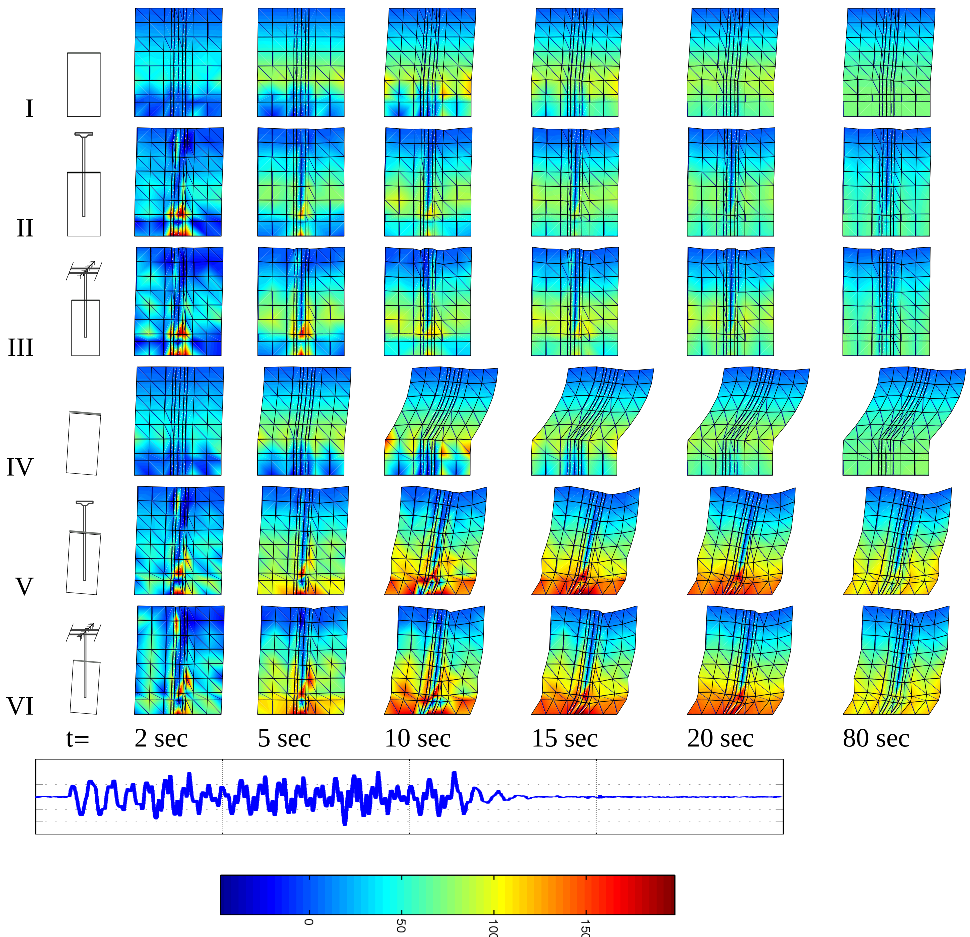

Figure 7: Time sequence of deformed shapes and excess pore pressure in symmetry plane of a soil system. Deformation is exaggerated 15 times; Color scale for excess pore pressures (above) is in kN/m^2. Graph of ground motions used (also shown in Figure (3)) is placed below appropriate time snapshots and is matching for $t = 2, 5, 10, 15, 20$ seconds while at $t = 80$ seconds there is no seismic shaking.

number of observation can be made on both deformation patterns, excess pore fluid patterns and their close coupling.

Level Ground without Pile (Case I).. Excess pore pressures and deformations in symmetry plane for level ground without a pile are shown in Figure (7) (I). At the very beginning (at $t = 2$ s) there is initial development of excess pore fluid pressure in the middle soil layers. This expected, as the self weight loading stage has densified lower soil layers enough so that their response is not initially contractive enough to produce excess pore pressure. Top soil layers, on the other hand, have a drainage boundary (top surface) too close to develop any significant excess pore pressures. As seismic shaking progresses (for $t = 5, 10$ s), the excess pore pressure increases, and starts developing in lower soil layers as well. It should be noted that a small non-uniformity in results is present. For example, zones of variable, nonuniform excess pore pressures on the lower mid and right side for Case I at $t = 10$ s develop. Nonuniform mesh (many small, long elements in the middle, large elements outside this middle zone) may introduce small numerical errors in results which can be observed by slightly nonuniform results at $t = 10$ s and $t = 15$ s. It should be noted that results for excess pore pressure shown for first 13 seconds (during shaking) in Figure (7) (I) are transient in nature, that is, seismic waves are traveling throughout the domain (model) during shaking (first 13 seconds) and slight oscillations in vertical stresses are possible. This oscillations will contribute to the (small) non-uniformity of excess pore pressure results. After the shaking (after 15 seconds) resulting excess pore pressure field is quite uniform.

Level Ground with Pile (Cases II and III).. Excess pore pressures and deformations in symmetry plane for models with PCM system and with two different boundary conditions at top of column (see model description in section 3.4) in level ground are shown in Figures (7) (II and III). One of the interesting observations is significant shearing and excess pore pressure generation adjacent to the pile tip. The reason for this is that pile is too short, that is, pile tip has significant horizontal displacements during shaking. Those pile tip displacements shear the soil, resulting in excess pore pressure generation. As soon as there is time for dissipation, this localized excess pore pressure dissipates to adjacent soil, and then, after shaking has ceased (at $t = 13$ s and later), it slowly dissipates upward. Addition of pile into the model (construction), with a highly impermeable elements (that mimic permeability of concrete) is apparent as there is a low excess pore pressure region in the middle of model, where pile is located.

Sloping Ground without Pile (Case IV).. Excess pore pressures and deformation in symmetry plane for sloping ground without pile is shown in Figures (7) (IV). It is noted that initially the excess pore pressure starts developing in middle soil layers,similar to the Case I above. Bottom layers start developing excess pore pressure only after significant shear deformation occurs (at $t = 10$ s) at approximately $2/3$ of the model depth. Lower layers have densified enough during self weight stage of loading that initial shaking is not strong enough to create excess pore water pressure, rather, those layers are fed by the excess pore pressure from above. Lower soil layers also do not develop much deformation, while middle and upper layers together develop excessive horizontal deformation.

Sloping Ground with Pile (Cases V and VI).. Excess pore pressures and deformation in symmetry plane for sloping ground with PCM system are shown in Figures (7) (V and VI). Similar to the above cases (II and III), pile is too short and there is again excessive shearing of soil at the pile tip, suggesting large movement of that pile tip. In addition to that, pile introduces significant stiffness to upper 12 meters of soil (along the length of pile) and helps reduce deformation of those upper soil layers. Down-slope gravity load is thus transferred to lower soil layers (below pile tip) which exhibit most of the deformation. It should be noted that soil in middle and upper layers (adjacent to pile) does deform, just not as much as the soil below pile tip. The predominant mode of deformation of middle soil layers is shearing in horizontal plane, around the pile. Deformation in horizontal plane is not significant as the pile is short in this examples (as mentioned above) and does not have enough horizontal support at the bottom. The deformation pattern of a soil – pile system is such that pile experiences significant rotation, and deforms with the soil that moves down-slope. If the pile was longer, and if it had significant horizontal support at the bottom, the middle and upper soil layers would have showed more significant flow around the pile in horizontal planes.

Upper layers undergo significant settlement, as seen in Figure (8). This settlement is mainly caused by the above mentioned rotation of pile–soil system, where soil in general settles (compacts) but also undergoes differential settlement, between left (up–slope from pile) and right (down–slope from pile) side of the model. As significant shearing with excess pore pressure generation develops in lower soil layers, below pile tip, those lower layers contribute to most of down–slope horizontal deformation. In a sense, all the demand from down-slope gravity forces and seismic shaking is now responded to by lower soil layers, which contribute to most of the excess pore pressure generation and consequently, to most of the soil deformation. Soil surface horizontal deformation is thus strongly influenced by significant shearing of the bottom layers and by rotation of the middle and upper soil layers with the pile. It is interesting to note

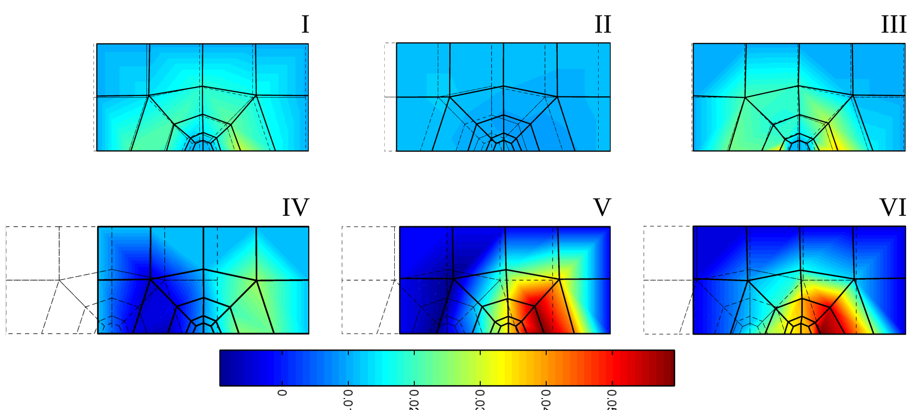

Figure 8: Soil surface settlements at 120 s for all six cases. Color scale given in meters

that the largest settlement is observed just down-slope from pile for Cases V and VI.

4.3. Pile Response

Figure (9) shows bending moment envelops for pile–column–mass (PCM) system for all four cases (II, III, V and VI). It should be noted that bending moment diagrams are plotted on compression side of the beam–column. A number of observations can be made about bending moment envelopes. For cases with free pile head (shaking transverse to the bridge main axes, Cases II and V) the maximum moments are attained in soil, at depths of approximately $0.6D - 1.2D$, where D (= 1.0 m in this case) is the pile diameter. Opposed to that are cases for PCM systems with restricted rotations at the pile top which (Cases III and VI), which, of course feature largest moment at the column top. Maximum bending moments for section of PCM system in soil (pile) in these two cases are now attained at the depth of approximately $1.8D - 2.0D$.

It is noted that bending moment envelopes are mostly symmetric. Slight non–symmetry is introduced for cases on sloping ground (Case V and VI). It is also noted that moments do exist (are not zero) all the say to the bottom of the pile. Theoretically, moments should be zero at the pile tip, but since physical volume of the pile is considered (see note on that in section 3.2 and Figure (2)), differential pressure on pile bottom from soil will produce small (non–zero) moments even at the pile tip. More importantly, non–zero moments at the bottom and along the lower part of the pile show that pile is indeed too short, and thus changing curvatures are present along the whole length of the pile.

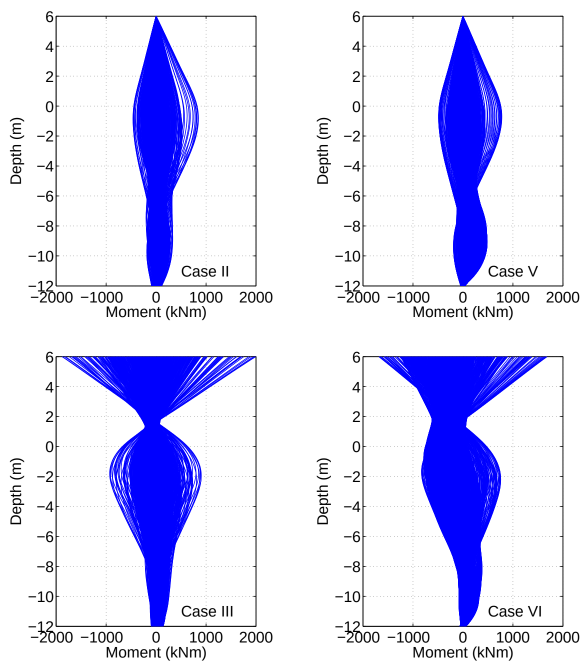

Figure 9: Envelope of bending moments for pile–column system for Cases II, III, V and VI.

4.4. Pile Pinning Effects

Piles in sloping liquefying ground can also be used to resists movement of soil (all liquefied or liquefied with hard crust on top) down–slope. For models developed in this paper, pile pinning effect can be investigated for Cases IV, V and VI. In particular, deformation of sloping ground without the pile (Case IV) can be compared with either of the cases of piles in sloping ground, Cases V and VI. It is very important to note, again, that models developed here had relatively short pile, and that major soil shearing developed below the pile tip. This apparent shortcoming of a short pile results in reduced pile pinning capacity, thus reducing the down–slope movement by only approximately half, from 0.35 m (Case IV) to 0.22 m (Case V) and to 0.18 m (Case VI) as seen in Figure (10). It would have been expected that, had the pile been longer and had it penetrated in deeper, non-liquefiable layers, it would have reduced down–slope movement of the soil to a much larger extent. However, had the pile been longer and had it penetrated non-liquefiable layers, it would have had a much firmer horizontal support at the bottom and would have thus attracted much larger forces too, potentially leading to pile damage and yielding.

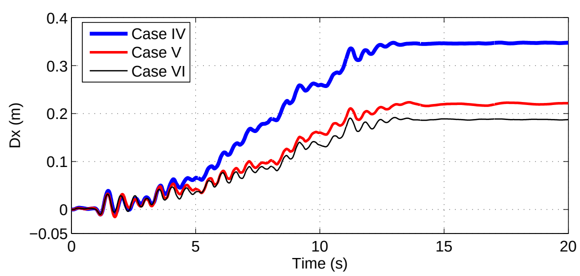

Figure 10: Down–slope movement at the ground surface (model center) for Cases IV (no pile), V and VI (with pile–mass system).

5. Summary

Presented in this paper was methodology for numerical modeling and simulation of piles in liquefiable soil. Of particular interest was the detailed description of modeling which aimed at replicating the prototype model as close as possible. High fidelity modeling included use of verified and validated models, detailed model development, including use of realistic loading stages. Detailed application of loading staged, starting from a zero state of stress and strain for a soil without a pile, followed by application of soil self weight, excavation and pile–column installation with application of pile–column self-weighting is finally followed by seismic loading with extended time after that for dissipation of excess pore pressures that have developed. An implementation for a bounding surface elastic–plastic sand model that accounts for fabric change, and for a fully coupled porous media (soil skeleton) – pore fluid (water) dynamic finite element formulation were developed and used in simulation of soil and water displacement and pore water pressure.

Six models were developed and simulated, feature level and sloping ground without and with pile–column systems. Results of simulations are presented with the aim of increasing our understanding of behavior of soil–pile–column systems during liquefaction events, including lateral soil deformation, effects of pile pinning, and ground settlement. In addition to detailed presentation of useful and interesting results, one of the main aims of this paper was to emphasize the need for, importance and availability of high fidelity modeling tools for simulating effects of liquefied soil on soil–structure systems.

Acknowledgment

Work presented in this paper was supported in part by the Earthquake Engineering Research Centers Program of the National Science Foundation under Award Number EEC-9701568.

References

Steven L. Kramer. Geotechnical Earthquake Engineering. Prentice Hall, Inc, Upper Saddle River, New Jersey, 1996.

Zhao Cheng, Mahdi Taiebat, Boris Jeremić, and Yannis Dafalias. Modeling and simulation of saturated geomaterials. In In proceedings of the GeoDenver conference, 2007.

Boris Jeremić, Zhao Cheng, Mahdi Taiebat, and Yannis F. Dafalias. Numerical simulation of fully saturated porous materials. International Journal for Numerical and Analytical Methods in Geomechanics, 32(13):1635–1660, 2008.

David Muir Wood. Geotechnical Modeling. Spoon Press, 2004. ISBN 0-415–34304.

Harry G. Harris and Gajanan M. Sabnis. Structural Modeling and Experimental Techniques. CRC Press, 1999. ISBN 0849324696.

T. L. Youd and S. F. Bartlett. Case histories of lateral spreads from the 1964 Alaskan earthquake. In Proceedings of the Third Japan–U.S. Workshop on Earth Resistant Design of Lifeline Facilities and Countermeasures for Soils Liquefaction, number 91-0001 in NCEER, Feb 1. 1989.

M. Hamada. Large ground deformations and their effects on lifelines: 1964 Niigata earthquake. In Hamada and O'Rourke, editors, Case Studies of Liquefaction and Lifeline Performance During Past Earthquakes, Vol 1: Japanese Case Studies, Chapter 3, pages 3:1 – 3:123, 1992.

Japanese Society of Civil Engineers. The report of damage investigation in the 1964 Niigata Earthquake. Japanese Soc. of Civil Engineers, Tokyo, 1966. in Japanese.

K. Yokoyama, K. Tamura, and O. Matsuo. Design methods of bridge foundations against soil liquefaction and liquefaction induced ground flow. In 2nd Italy–Japan Workshop on Seismic Design and Retrofit of Bridges, page 23 pages, Rome, Italy, 27-28 Feb. 1997.

J. B. Berril, S. A. Christensen, R. J. Keenan, W. Okada, and J. K. Pettinga. Lateral–spreading loads on a piled bridge foundations. In Seco E. Pinto, editor, Seismic Behavior of Ground and Geotechnical Structures, pages 173–183, 1997.

Ricardo Dobry and Tarek Abdoun. Recent studies on seismic centrifuge modeling of liquefaction and its effects on deep foundations. In S. Prakash, editor, Proceedings of Fourth International Conference on Recent Advances in Geotechnical Earthquake Engineering and Soil Dynamics, San Diego, March 26-31 2001.

Japanese Road Association. Specification for highway bridges, 1980.

Architectural Institutive of Japan. Recomendation for design of building foundations, 1988.

L. Liu and R. Dobry. Effect of liquefaction on lateral response of piles by centrifuge model tests. In NCEER Bulletin, volume 9:1, pages 7–11. National Center for Earthquake Engineering Research, January 1995.

F. Miura, H. E. Stewart, and T. D. O'Rourke. Nolinear analysis of piles subjected to liquefaction induced large ground deformation. In Proceedings of the Second U.S.–Japan Workshop on Liquefaction , Large Ground Deformations and Their Effect on Lifelines, number 0032 in NCEER-89, Sept. 26-29 1989.

F. Miura T. D. O'Rourke. Lateral spreading effects on pile foundations. In Proceedings of the Third U.S.–Japan Workshop on Earthquake Resistant Design of Lifeline Facilities and Countermeasures for Soil Liquefaction, number 0001 in NCEER-91, Feb. 1 1991.

K.–I. Tokida, H. Matsumoto, and H. Iwasaki. Experimental study of drag action of piles in ground flowing by liquefaction. In Proceedings of Fourth Japan–U.S. Workshop on Earthquake Resistant Design of Lifeline Facilities and Countermeasures for Soil Liquefaction, volume 1 of NCEER92-0019, SUNY Buffalo, N. Y., 1992.

T. Abdoun, R. Dobry, and T. D. O'Rourke. Centrifuge and numerical modeling of soil–pile interaction during earthquake induced soil liquefaction and lateral spreading. In Geotechnical Special Publications 64, pages 76–90. ASCE, 1997.

K. Horikoshi, A/ Tateishi, and T. Fujiwara. Centrifuge modeling of single pile subjected to liquefaction-induced lateral spreading. Soils and Foundations, Special Issue(2):193–208, 1998.

R. W. Boulanger and K. Tokimatsu, editors. Seismic Performance and Simulation of Pile Foundations in Liquefied and Laterally Spreading Ground. Geotechnical Special Publication No 145. ASCE Press, Reston, VA, 2006. 321 pp.

K. Tokimatsu and Y. Asaka. Effects of liquefaction–induced ground displacements on pile performance in the 1995 hyogoken–nambu earthquake. Special Issue of Soils and Foundations, Japanese Geotechnical Society, pages 163–177, 1998.

G. R. Martin, M. L. March, D. G. Anderson, R. L. Mayes, and M. S. Power. Recommended design approach for liquefaction induced lateral spreads. In Proceedings of the 3rd National Seismic Conf and Workshop on Bridges and highways, MCEER–02–SP04, Buffalo, NY, 2002.

R. Dobry, T. Abdoun, T. D. ORourke, and S. H. Goh. Single piles in lateral spreads: Field bending moment evaluation. Journal of Geotechnical and Geoenvironmental Engineering, 129(10):879–889, 2003.

D. S. Liyanapathirana and H. G. Poulos. Pseudostatic approach for seismic analysis of piles in liquefying soil. Journal of Geotechnical and Geoenvironmental Engineering, 131(12):1480–1487, 2005.

K. M. Rollins, T. M. Gerber, J. D. Lane, and S. A. Ashford. Lateral resistance of a full–scale pile group in liquefied sand. Journal of Geotechnical and Geoenvironmental Engineering, 131(1):115–125, 2005.

M. Čubrinovski and K. Ishihara. Assessment of pile group response to lateral spreading by single pile analysis. In Seismic Performance and Simulation of Pile Foundations in Liquefied and Laterally Spreading Ground, Geotechnical Special Publication No. 145, pages 242–254. ASCE, 2006.

S. J. Brandenberg, R. W. Boulanger, B. L. Kutter, and D. Chang. Static pushover analyses of pile groups in liquefied and laterally spreading ground in centrifuge tests. Journal of Geotechnical and Geoenvironmental Engineering, 133(9):1055–1066, 2007.

R. V. Whitman. On liquefaction. In Proceedings of the 11th Int. Conf. on Soil Mechanics and Foundation Engineering, pages 1923–1926, San Francisco, 1985. Balkema, Rotterdam, The Netherlands.

National Research Council. Liquefaction of soils during earthquakes. National Academy Press, Washington, D.C., 1985.

Erik J. Malvick, Bruce L. Kutter, Ross W. Boulanger, and R. Kulasingam. Shear localization due to liquefaction–induced void redistribution in a layered infinite slope. ASCE Journal of Geotechnical and Geoenvironmental Engineering, 132(10):1293–1303, 2006.

Arthur Casagrande and Franklin Rendon. Gyratory shear apparatus; design, testing procedures. Technical Report S–78–15, U.S. Army Corps of Engineers, Waterways Experiment Station, Vicksburg, Miss., 1978.

P. A. Gilbert. Investigation of density variation in triaxial test specimens of cohesionless soil subjected to cyclic and monotonic loadin. Technical Report GL–84–10, U.S. Army Corps of Engineers, Waterways Experiment Station, Vicksburg, Miss., 1984.

O. C. Zienkiewicz and T. Shiomi. Dynamic behaviour of saturated porous media; the generalized Biot formulation and its numerical solution. International Journal for Numerical Methods in Engineering, 8:71–96, 1984.

O. C. Zienkiewicz and R. L. Taylor. The Finite Element Method, Volume 1, The Basis, 5th Edition. Butterworth Heinemann, London, 2000.

Ahmed Elgamal, Zhaohui Yang, and Ender Parra. Computational modeling of cyclic mobility and post–liquefaction site response. Soil Dynamics and Earthquake Engineering, 22:259–271, 2002.

Ahmed Elgamal, Zhaohui Yang, Ender Parra, and Ahmed Ragheb. Modeling of cyclic mobility in saturated cohesionless soils. International Journal of Plasticity, 19(6): 883–905, 2003.

Jean H. Prevost. Wave propagation in fluid-saturated porous media: an efficient finite element procedure. Soil Dynamics and Earthquake Engineering, 4(4):183 –202, 1985.

Andrew Hin-Cheong Chan. A Unified Finite Element Solution to Static and Dynamic Problems in Geomecahnics. PhD thesis, Department of Civil Engineering, University College of Swansea, February 1988.

O.C. Zienkiewicz, A.H.C. Chan, M. Pastor, B.A. Schrefler, and T. Shiomi. Computational Geomechanics–with Special Reference to Earthquake Engineering. John Wiley and Sons Ltd., Baffins Lane, Chichester, West Sussex PO19 IUD, England, 1999.

M. Pastor, O. C. Zienkiewicz, and A. H. C. Chan. Generalized plasticity and the modeling of soil behaviour. International Journal for Numerical and Analytical Methods in Geomechanics, 14:151–190, 1990.

John Argyris and Hans-Peter Mlejnek. Dynamics of Structures. North Holland in USA Elsevier, 1991.

N. M. Newmark. A method of computation for structural dynamics. ASCE Journal of Engineering Mechanics Division, 85:67–94, 1959.

H. M. Hilber, T. J. R. Hughes, and R. L. Taylor. Improved numerical dissipation for time integration algorithms in structural dynamics. Earthquake Engineering and Structure Dynamics, pages 283–292, 1977.

T. J. R. Hughes and W. K. Liu. Implicit-explicit finite elements in transient analaysis: implementation and numerical examples. Journal of Applied Mechanics, pages 375–378, 1978a.

T. J. R. Hughes and W. K. Liu. Implicit-explicit finite elements in transient analaysis: stability theory. Journal of Applied Mechanics, pages 371–374, 1978b.

Anil K. Chopra. Dynamics of Structures, Theory and Application to Earhquake Engineering. Prentice Hall, second edition, 2000. ISBN 0-13-086973-2.

Thomas J. R. Hughes. The Finite Element Method ; Linear Static and Dynamic Finite Element Analysis. Prentice Hall Inc., 1987.

M. T. Manzari and Y. F. Dafalias. A critical state two–surface plasticity model for sands. Géotechnique, 47(2):255–272, 1997.

Yannis F. Dafalias and Majid T. Manzari. Simple plasticity sand model accounting for fabric change effects. Journal of Engineering Mechanics, 130(6):622–634, 2004.

William L. Oberkampf, Timothy G. Trucano, and Charles Hirsch. Verification, validation and predictive capability in computational engineering and physics. In Proceedings of the Foundations for Verification and Validation on the 21st Century Workshop, pages 1–74, Laurel, Maryland, October 22-23 2002. Johns Hopkins University / Applied Physics Laboratory.

Olivier Coussy. Mechanics of Porous Continua. John Wiley and Sons, 1995. ISBN 471 95267 2.

A. Gajo. Influence of viscous coupling in propagation of elastic waves in saturated soil. ASCE Journal of Geotechnical Engineering, 121(9):636–644, September 1995.

A. Gajo and L. Mongiovi. An analytical solution for the transient response of saturated linear elastic porous media. International Journal for Numerical and Analytical Methods in Geomechanics, 19(6):399–413, 1995.

Olgierd Cecil Zienkiewicz and Robert L. Taylor. The Finite Element Method, volume 1. McGraw - Hill Book Company, fourth edition, 1991a.

Olgierd Cecil Zienkiewicz and Robert L. Taylor. The Finite Element Method, volume 2. McGraw - Hill Book Company, Fourth edition, 1991b.

J. E. Dennis, Jr. and Robert B. Schnabel. Numerical Methods for Unconstrained Optimization and Nonlinear Equations. Prentice Hall , Engelwood Cliffs, New Jersey 07632., 1983.

Ramon Verdugo and Kenji Ishihara. The steady state of sandy soils. Soils and Foundations, 36(2):81–91, 1996.

E. Spacone, F. C. Filippou, and F. F. Taucer. Fibre beam-column model for non-linear analysis of r/c frames: Part i. formulation. Earthquake Engineering & Structural Dynamics, 25(7):711–725, July 1996a.

E. Spacone, F. C. Filippou, and F. F. Taucer. Fibre beam-column model for non-linear analysis of r/c frames: Part ii. applicationss. Earthquake Engineering & Structural Dynamics, 25(7):727–742, July 1996b.

Kandiah Arulanandan and Ronald F. Scott, editors. Verification of Numerical Procedures for the Analysis of Soil Liquefaction Problems. A. A. Balkema, 1993.

M. Čubrinovski, R. Uzuoka, H. Sugita, K. Tokimatsu, M. Sato, K. Ishihara, Y. Tsukamoto, and T. Kamata. Prediction of pile response to lateral spreading by 3-d soil–coupled dynamic analysis: Shaking in the direction of ground flow. Soil Dynamics and Earthquake Engineering, 28(6):421–435, June 2008.

R. Uzuoka, M. Čubrinovski, H. Sugita, M. Sato, K. Tokimatsu, N. Sento, M. Kazama, F. Zhang, A. Yashima, and F. Oka. Prediction of pile response to lateral spreading by 3-d soil–coupled dynamic analysis: Shaking in the direction perpendicular to ground flow. Soil Dynamics and Earthquake Engineering, 28(6):436–452, June 2008.

T. Sakemi, M. Tanaka, Y. Higuchi, K. Kawasaki, and K. Nagura. Permeability of pore fluids in the centrifugal fields. In 10th Asian Regional Conference on Soil Mechanics and Foundation Engineering (10ARC), Beijing, China, August 29 - Sept 2 1995.

Miško Čubrinovski. Private communications. ..., 2007 –.